Low temperature, pressureless sp2 to sp3 transformation of ultrathin, crystalline carbon films

Fabrice Piazza, Kathleen Gough, Marc Monthioux, Pascal Puech, I.C. Gerber, Richard Wiens, Germercy Paredes, Cristhofer Ozoria

Low temperature, pressureless sp^2 to sp^3 transformation of ultrathin, crystalline carbon films

Fabrice Piazza[1*], Kathleen Gough[2], Marc Monthioux[3], Pascal Puech[3], Iann Gerber[4], Richard Wiens[2], Germercy Paredes[1], Cristhofer Ozoria[1]

[1] Nanoscience Research Laboratory, Pontificia Universidad Católica Madre y Maestra, Autopista Duarte km 1 1/2, Apartado Postal 822, Santiago, Dominican Republic

[2] Department of Chemistry, Universidad de Manitoba, Winnipeg, Canada

[3] Centre d'Elaboration des Matériaux et d'Etudes Structurales (CEMES), CNRS, Université de Toulouse, France

[4] Laboratoire de Physico-Chimie des Nano-Objets (LPCNO), CNRS, INSA, Université de Toulouse, France

Abstract

Nanosized and crystalline sp^3-bonded carbon materials were prepared over large surface areas up to ~33x51 μm^2 from the exposure of few-layer graphene (FLG) to H radicals produced by the hot-filament process at low temperature (below 325 °C) and pressure (50 Torr). Hybrid materials were also obtained from the partial conversion of FLG. sp^3-C related peaks from diamond and/or lonsdaleite and/or hybrids of both were detected in UV and visible Raman spectra. C-H bonding was directly detected by Fourier Transform Infrared (FTIR) microscopy over an area of ~150 μm^2 and one single component attributed to sp^3-C-H mode was detected in the C-H stretching band showing that carbon is bonded to one single hydrogen and strongly suggesting that the sp^3-C materials obtained are ultrathin films with basal planes hydrogenated. The experimental results are compared to computational predictions and comprehensively discussed. Those materials constitute new synthetic carbon nanoforms after fullerenes, nanodiamonds, carbon nanotubes and graphene. This opens the door to new research in multiple areas for the development of new potential applications and may have wide scientific impact, including for the understanding of extraterrestrial diamond-related structures and polytype formation mechanism(s).

*Corresponding author. E-mail: fpiazza75@gmail.com; fpiazza@pucmm.edu.do (Fabrice Piazza)

1. Introduction

Beyond graphene, a new nanocrystalline carbon material consisting of few atomic layers (FL) of diamond or lonsdaleite, also called diamane by Chernozatonskii et al. who first predicted it [1], holds great technological promise and is attracting increasing interest [1,2,3,4,5,6,7,8,9,10,11,12,13,14,15,16,17,18]. In such a material, sp^3-bonded carbon atoms are arranged in a hexagonal lattice. According to calculations, such sheets would be produced by the chemisorption of hydrogen atoms on the "top" and "bottom" surfaces of two- or three-layer graphene and the subsequent interlayer sp^3-C bond formation [1,2,3]. Another possibility would be the conversion of few-layer graphene (FLG) on a metal surface into a sp^3-carbon film through hydrogenation of the top layer. In this case, strong hybridization between the sp^3 dangling bond orbitals and the metallic surface orbitals would stabilize the sp^3-bonded carbon layers [11,12]. A last approach, which is not explored in the present work, would be the use of high pressure to induce the sp^2-to-sp^3 transformation [5,15,16].

A single layer of diamane refers to the full hydrogenation of a single graphene, a material known as graphane, which was tentatively prepared in Ref. [19]. The stability of graphane was first predicted by Soto et al [20]. Graphane consists of a single layer of hexagonal network of sp^3-bonded carbon in which every carbon is bonded to hydrogen, alternately above and below the layer. The synthesis of graphane remains elusive. In ref. [19] full hydrogenation was not achieved as evidenced in the published Raman spectra which contain sp^2-C features. The authors in Ref [19] claim that a small residual sp^2 phase dominates their spectra because of the much larger Raman diffusion cross-section for sp^2-carbon than for sp^3-carbon. However, in fully fluorinated graphene, a material known as fluorographene, sp^2-C features are not observed in visible Raman spectra [21]. Graphane could be considered as the first member in the series of diamanes of increasing thickness, as a new class of carbon nanoform which nomenclature is not consensual yet. The chemically-induced phase conversion of FLG into a C(sp^3) structure may have been previously obtained from the chemisorption of halogen atoms such as fluorine [22]. However, to the best of authors' knowledge, diamane structure has not been evidenced.

According to computational studies, diamanes display the electronic structure of semiconductors, with a direct band-gap depending on the film thickness, which make them very attractive for nanoelectronics, band-gap engineering and active laser medium in nanooptics [4,7]. Because of their expected high thermal conductivity, they may also be used in thermal management

devices [10]. Furthermore, the incorporation of nitrogen-vacancy (N-V) centers in diamanes through substitution by nitrogen atoms in the C lattice could be used to configure qbits for use in quantum computing [10]. Diamanes are also expected to be very strong, which would make them very attractive for ultrathin protective coatings, ultrahigh-strength components in composite materials for aerospace applications for instance, and nano-electromechanical systems [10]. Because of the expected low friction coefficient of the hydrogenated surface, diamanes may also be used to improve the wear resistance of coated mechanical parts. In addition, diamanes are expected to be biocompatible, so that they may become very important component in bio-devices and bio-sensors. Heterostructures of graphene and diamane would be attractive for tunnel devices, optical linear waveguides, high efficiency optoelectronic sensors, lithium batteries, and supercapacitors [4,10]. Finally, mass production of few layer lonsdaleite, in particular from a low pressure method, would be very desirable for protective thin film and composite materials in mechanical applications, as it is predicted that lonsdaleite is 58 % harder than diamond [23]. It was claimed once that "*lonsdaleite is faulted and twinned cubic diamond and does not exist as a discrete material*" [24]. However, this statement was based on the analysis by transmission electron microscopy, at a rather high energy of 200 keV (hence likely to modify the material), of only two non-pure samples, a natural one and a synthetic one. It was also based on the observation that no example of successful synthesis of lonsdaleite was reported in the literature. Therefore, the demonstration is weak. In the absence of any reason why lonsdaleite could not form as an isolated phase, the possibility that suitable conditions could be found one day cannot be excluded. A very similar case can be found with rhombohedral graphite, usually found as stacking faults in hexagonal graphite but which existence as an isolated phase was claimed impossible for decades, until the contrary demonstration was made [25].

Even if various studies based on calculations hypothesized that diamane can form when non-supported 2LG and 3LG are placed in hydrogen cold plasma, to the best of authors' knowledge, there is no report of any experimental evidence of such scenario. Only few experimental studies on the hydrogenation of FLG have been published [19,26,27,28,29]. In particular, no features from diamane were reported in Raman spectra. Rajasekaran *et al.* reported on carbon-carbon interlayer bond formation in FLG up to 4 layers through deuterium adsorption on FLG surface which resulted in a thin film of diamond-like layer on a Pt(111) substrate as evidenced by synchrotron spectroscopic techniques [12]. The surface adsorption of H induced a hybridization change of carbon from the sp^2 to the sp^3 bond symmetry, which propagated through the graphene layers, resulting in interlayer

carbon bond formation. According to the authors of Ref. [12], the structure was stabilized through the termination of interfacial sp^3-C by the substrate. The structural transformation was believed to occur as a consequence of high adsorption energy. This would be in good agreement with the calculations of ref. [11]. However, crystal structure was not evidenced in ref. [12]. No Raman spectroscopy nor electron diffraction results were reported. The material obtained in ref. [12] could be sp^3-C-rich amorphous carbon, that is to say tetrahedral amorphous carbon (ta-C) [30,31]. Further work is necessary to evidence, understand and control diamane synthesis. In particular, it is not clear whether a metallic substrate is necessary or not to stabilize sp^3 bonding in hexagonal lattice.

To achieve the above-presented route to convert FLG into diamane, it is necessary to develop an efficient method to hydrogenate FLG. Yet, since the first experimental description of hydrogenated 1LG and 2LG [32], only few experimental studies and methods were reported on this topic. Those methods have been mainly focusing on two approaches: gas phase [19,26,27,29,33,34,35,36,37,38,39,40] or liquid phase hydrogenation [41,42,43,44,45,46]. A review on the subject is available in Ref. [47]. In any case, partially hydrogenated graphene has been prepared; never graphane. The liquid phase hydrogenation methods can generate a maximum of ~76 at.% of hydrogenated carbon atoms [41] against ~10 at.% in the gas phase methods [37]. Even though they have so far not lead to the highest hydrogenation rate, gas phase hydrogenation methods, especially at low temperature and low pressure, remain very attractive on a technology standpoint, in particular in applications where the use of wet-chemistry methods is limited, such as in nanoelectronics, where hydrogenation must be precisely and spatially controlled in a tunable manner. The hot-filament process may constitute a very competitive method for the efficient hydrogenation of FLG and the potential formation of diamane. It has been widely and preferentially used at industrial scale for the elaboration of microcrystalline and nanocrystalline diamond [48,49,50]. It has been developed to efficiently produce atomic hydrogen (H), which has been shown to play a critical role for the conventional synthesis of metastable diamond at low pressure from a dilute mixture of a hydrocarbon in H_2 [48,51,52,53]. H is produced heterogeneously by the thermal decomposition of H_2 on the hot filament surface, and then rapidly diffuses into the bulk gas. H recombination reactions are sufficiently slow at the typical process pressures (below 100 Torr) that most of the H diffuse to the reactor walls. H is present at super-equilibrium concentration throughout most of the reactor [53]. The effects of H_2 pressure and flow rate, filament temperature and radial distance from the filament on the relative H concentrations, and the gas temperature profiles were investigated in details, in particular for the case of pure H_2 [53,54,55,56,57,58,59]. In the hot

filament process, as compared to low pressure plasma techniques, the presence of ions accelerated toward the substrate and which can damage the graphene is avoided. Indeed, high kinetic energy ions in the plasma tend to etch the graphene film instead of participating in the hydrogenation process [37]. Besides, the hot filament process was used to grow crystalline nanodiamonds at low substrate temperature, below 300 °C [60,61,62]. It was used to coat carbon nanotube bundles with diamond and SiC nanocrystals from solid carbon and silicon sources exposed to H at around 190 °C [63,64]. The synthesis of hydrogenated graphene by the hot filament process onto a 1000 °C-heated copper substrate and from a gas mixture of CH_4:H_2 was previously reported [40]. However, this was evidenced by Raman spectroscopy analysis, which is ambiguous as detailed below.

One important aspect to achieve an efficient hydrogenation of FLG and subsequent conversion into crystalline sp^3-bonded C sheets is the choice of characterization techniques to unambiguously evidence C-H and sp^3-C-sp^3-C bonding. As pointed out in Ref. [47], only few studies [39,41,42,43,45] reported direct quantitative data on hydrogenation rate from reliable techniques such as combustion elemental analysis (CHNO) or nuclear magnetic resonance. This may be due to the small amount of material processed in most cases. Furthermore, only a few studies [27,39,41,42,43,44,45] reported on the direct detection of C-H bonding from Fourier transform infrared spectroscopy (FTIR), which is a highly sensitive and widely accessible technique. The lack of quantitative data and FTIR analysis characterizes most of the reports on gas phase hydrogenation methods. Those studies only rely on Raman spectroscopy analysis. However, Raman spectroscopy is an indirect method to detect C-H bonding since it probes indiscernibly any kind of defects; vacancies, edges and C-H bonding [19]. In some of those studies, the fact that all of the defect-related peaks in Raman spectra are suppressed or highly attenuated upon annealing or laser irradiation of hydrogenated graphene materials is used to show that defects generated during the hydrogenation treatment are C-H bonding [19]. However, Raman spectroscopy using single-point measurement cannot determine whether H is bonded to the surface of the layers or only to the edges. To the authors' knowledge, this last paramount point has not been addressed in the literature. Likewise, there is no Raman mapping analysis published for hydrogenated graphene while such analysis has been widely used for graphene research. Empirical analysis of Raman D and G peak intensity ratio from unknown number of single-point measurements has been used to estimate hydrogenation rates [37]. As far as we can tell, there is no FTIR mapping data published either. These are the reasons why it has been decided here to use Raman and FTIR mapping. Furthermore, as for visible energies, the Raman scattering of sp^2-C is a resonant process between 50 and 230 times

more effective than that of sp^3-C [65], Raman spectroscopy at 244 nm was employed to obtain a more evenly weighted probe of sp^3-C and sp^2-C sites. A review of the literature shows that there is a lack of understanding of the hydrogenation mechanisms of 1LG and FLG. There are contradictory results and interpretation concerning differences in reactivity for 1LG and FLG [19,26,32,36,38,28,29]. Hence, it is impossible to compare the results published so far. This is due to differences regarding the graphene materials, substrates, method and conditions used for the hydrogenation. Also, various studies lack of direct detection of C-H bonding and all fail to show that hydrogen is effectively bonded to basal plane.

In this work, we studied the hydrogenation of FLG by the chemisorption of H generated from the dissociation of H_2 in a hot filament reactor at low temperature and low pressure, and the subsequent FLG structure conversion into a crystalline sp^3 material. FTIR microscopy was used to track the formation of C-H bonds, and visible and UV Raman spectroscopy and mapping were used to track the structure conversion and the extension of the converted domains. We provide, for the first time, evidences of the crystalline structure of the sp^3-carbon material obtained from the hydrogenation of FLG at low temperature and at low pressure.

2. Experimental

2.1. Graphene pristine materials

As-received CVD FLG films deposited on 3 mm copper transmission electron microscopy (TEM) grids (2000 Mesh) from Graphene Supermarket (SKU # SKU-TEM-CU-2000-025) were used as graphene materials. The FLG films had been grown by CVD from CH_4 at 1000°C on Ni substrate and transferred onto a commercial TEM grid using a polymer-free transfer method to minimize contamination as described in Ref. [66]. FLG thickness is typically between 0.3-2 nm (1-6 monolayers), however thicker film, up to 20 layers, were observed in TEM. Typical FLG TEM grid coverage is between 60 and 90 %. For some control experiments, as-received bilayer graphene (2LG) deposited on 2.5 μm holey silicon nitride TEM grids from Ted Pella (PELCO® 2 Layer Graphene Prod No. 21722-10) was used as graphene material.

2.2. Hydrogenation process

A commercial hot filament reactor from Blue Wave Semiconductors (BWI 1000 model) previously described in details [63], was used for hydrogenation and subsequent structure conversion of FLG into ultrathin and crystalline sp^3-bonded carbon sheets. Briefly the reactor is a six-way cross stainless steel vacuum chamber. It is fluid-cooled (15% water, 75% glycol at 18 °C) with brazed copper tubing covered with an aluminum foil. The reactor is equipped with a molybdenum filament cartridge that accommodates between one and three 0.5 mm diameter straight metallic wires. In this study, two 5.7 cm length tungsten wires, 1 cm apart, were used. Prior mounting, the filaments were cleaned with acetone to avoid any carbon contamination. Substrates were placed on the movable and fluid-cooled 5 cm diameter stainless steel sample stage. FLG grids were placed vertically on the substrate holder and were pinched by two (100) silicon pieces (500-550 Ωm thickness, 14 mm x 14 mm) to keep their position fixed during operation. The silicon pieces were previously cleaned in an ultrasound acetone bath for 5 minutes, rinsed in deionized water, and dried in nitrogen at room temperature. The substrate holder and FLG temperatures were estimated by a thermocouple tip (K-type; sheathed wires) located on top of the surface of the substrate holder located in front of the filaments. Before synthesis, the reactor was evacuated down to 10^{-1} Torr (0.133 mbar) using a hydrocarbon oil pump (DUO 20M from Pfeiffer Vacuum). For hydrogenation, ultra-high purity H_2 gas (about 99.999 % pure) was introduced into the chamber via a stainless steel tube located on top of the chamber. Gas flow was regulated by an Omega mass flow controller. The pressure was regulated via an automatic valve located below the substrate holder. Once H_2 was introduced into the chamber and steady-state conditions were reached, the current for both filaments was raised and maintained at 55 A, which resulted in a filament temperature of 2330 °C, as monitored with a two-color pyrometer (M90R2 model from Mikron Infrared, Inc.). The pressure and flow were 50 Torr and 1 sccm, respectively. Before hydrogenation process, the tungsten filaments were not exposed to hydrocarbon gas for carburization or conditioning as it is necessary for the conventional growth of diamond by hot filament CVD. This was to avoid carbon contamination from a carburized filament. The distance between the substrate holder and the filaments was 22.8 mm. The resulting maximum substrate holder temperature was ~300°C. Taking into account substrate holder temperature variation with the distance between the substrate and the filaments, the maximum FLG temperature was ~325 °C, due to the closer proximity of the TEM grid substrate to the filaments. The duration of the hydrogenation process was 6 minutes and 20 seconds.

2.3. Material characterization

Multi-wavelength Raman spectroscopy was employed to examine the material structure before and after hydrogenation. Raman spectra were recorded with two Renishaw InVia Reflex Spectrometer Systems equipped with a stigmatic single pass spectrograph including holographic gratings of 2400 grooves.mm^{-1} (for visible analysis) and 3600 grooves.mm^{-1} (for UV analysis) and using the 244, 488 and 514.5 nm lines of Ar ion lasers. For the UV analysis, a 85 Lexel Second Harmonic Generation laser was employed. The scattered light was collected in the 180° backscattering geometry. For visible analysis, a ×50 objective was used while for UV analysis, a ×40 objective was employed. For UV Raman spectroscopy, the detection system was a Peltier-cooled UV coated Deep Depletion CCD array detector and the entrance slit was set to 50 μm. The resolution was of 1 cm^{-1}. The laser power on the sample and acquisition time were adjusted to obtain optimum signal without any sample modification. Typically, laser power was in the range of 1 mW, and exposure time to the laser was in the range of 1 s. No visible damage and no change of the spectral shape during measurements have been observed unless exposure time was intentionally raised to induce some structure modification in specific experiments as detailed below. Silicon and highly-oriented pyrolytic graphite (HOPG) were used for peak position calibration: silicon for spectra excited with visible radiation, and HOPG for spectra excited with deep UV radiation. Raman mapping was employed using high-speed encoded mapping stage and a 1" CCD to generate high definition 2D chemical images over thousands of square microns. Probed surface area was typically of ~140×100 μm^2. Peaks were fitted using Lorentzian function using Wire 4.4 software from Renishaw.

C-H bonding was directly detected using Fourier Transform Infrared (FTIR) spectroscopy. FTIR images and spectra were recorded with an Agilent Technologies Cary 670 FTIR spectrometer coupled to a Cary 620 FTIR microscope equipped with a 64×64 focal plane array mercury cadmium telluride detector. Attenuated Total Reflection (ATR) mode, with a germanium crystal as internal reflection element, was employed.

It is worth noting that the converted material, as opposed to the behavior of graphene or diamond, appeared to be electron sensitive, possibly because of the high hydrogenation degree of the surface, even for electron energy as low as 80 keV. Therefore, attempts of TEM-related investigation (including electron diffraction and EELS) could not be conclusive and will not be shown.

2.4. Computational Details

The atomic structures, the quasi-particle band structures and optical spectra were obtained from Density Functional Theory calculations using the VASP package [67,68] and the plane-augmented wave scheme [69,70] to treat core electrons. Perdew-Burke-Ernzerhof (PBE) functional [71] was used as an approximation of the exchange-correlation electronic term for all the geometry optimization steps as well as for phonons and frequencies calculations. The cut-off energy was set to 400 eV, with a Gaussian smearing with a width of 0.05 eV for partial occupancies. To build the wave-function, which served as starting point for further G_0W_0 calculations [72,73], the Heyd-Scuseria-Ernzerhof (HSE) exchange-correlation functional [74,75] was used. During geometry optimization step all the atoms were allowed to relax with a force convergence criterion below 0.005 eV/Å. The optimized lattice parameter of graphane, bilayer-diamane and three-layer diamane were 2.53, 2.52 and 2.52 Å, respectively. A vacuum height of 20 Å was used to avoid spurious interaction between periodic images of the different slabs. A 21x21x1 grid was set for G_0W_0 calculations, in conjunction with a total number of bands of 800, and an energy cutoff of 100 eV for the response function, after a careful check of the direct band-gap convergence, to be smaller than 0.1 eV in function of k-points sampling. To estimate phonon dispersion (7x7) supercells were used with a 3x3x1 grid for k-points sampling, in the Density Functional Perturbation Theory (DFPT) framework, using the Phonopy code [76]. C-H stretching mode frequency calculations were performed from a finite difference approach and using a displacement of 0.001 Å.

2.5. Nomenclature

Although diamane has been described as a full series of materials structurally derived from hydrogenated bilayer graphene (2LG), the first structure that the hydrogenation of a graphene could form is actually graphane, which consists of a single layer of a hexagonal network of sp^3-bonded carbon atoms in which each carbon is bonded to one hydrogen atom, alternately above and below the layer. Then comes genuine diamane, which should be limited to the two-layer structure strictly speaking, i.e., where half of the carbons from the top layer are hydrogenated while the other half is bonded to carbon atoms from the bottom layer, in which, consequently, only half of the carbon atoms are hydrogenated as well. Two structural configurations are possible, depending on whether the

stacking sequence in the starting 2LG is AB or AA. The former will result in the diamond structure-based diamane (called diamane I in [1]), while the latter will result in the lonsdaleite structure-based diamane (called diamane II in [1]). As the number of layers increases, because the inner layers cannot be hydrogenated, diamane-related materials should be more accurately described as surface-hydrogenated diamond or lonsdaleite, or more generally diamanoïds, in order to include any mixture of diamond polytypes. However, whereas an AB 2LG can generate a diamond structure, an ABA 3LG cannot. But the diamond structure can develop from ABCAetc. (i.e., the stacking sequence of rhombohedral graphite). On the other hand, lonsdaleite structure can develop from AAA… stacking. As soon as a diamanoïd is built from more than 2 graphenes, its structure can also result from a mixture of diamond and lonsdaleite. Because of this, beside graphane and diamane (I and II), it is more relevant to designate the subsequent hydrogenated multilayer diamanoïd structures with the number of layers equal to 3, 4 and so on up to "few", by the stacking sequence of the starting graphenes, as suggested in [4], for instance (ABB)D, (ABBA)D, (ABBC)D, (AABBCC)D, and so on (where “D” stands for “Diamanoïd”). Alternatively, as for graphene, mention could be made of the number of stacked layers without precising the stacking sequence, i.e., 3LD, 4LD, 5LD and so on up to FLD or MLD (where F/MLD stands for “few/multi-layer diamanoïd”). What the limit of "few" is cannot be given so far, because calculations for showing above which number of layers diamanoïd properties no longer discriminate from regular diamond or lonsdaleite are yet to be performed. It is worth noting that this nomenclature does not discriminate whether one surface or both (i.e., top and bottom layers) are hydrogenated. In case it is necessary, 1H-FLD and 2H-FLD could be used to designate one-surface- and both-surface-hydrogenated few-layer diamanoïd, respectively. Likewise, in some conditions, hydrogenation may affect one surface only of the two-layer C(sp^3) structure (AB or AA), hence it is no longer genuine diamane. In such a case, this material may be described as “surface hydrogenated 2-layer diamond or lonsdaleite”, which may be abbreviated as 1H-2D or 1H-2L, respectively. If fluorination is concerned instead of hydrogenation, “H” can then be substituted by “F” in the proposed nomenclature. Likewise for any other atom or functional group the surface carbon atoms could be bonded to instead of H.

3. Results and discussion

3.1. Visible Raman spectroscopy

Different types of spectra were obtained for a given sample. It is supposed that this is due to the variation in the number of layers, their respective orientation and the subsequent variation in hydrogenation rate [19,26,32]. FIG. 1B shows a typical Raman spectrum obtained after H exposure taken at 488 nm. FIG. 1A shows the spectrum before hydrogenation for comparison, which is typical from pristine FLG [77]. It shows the G and 2D peaks [77].

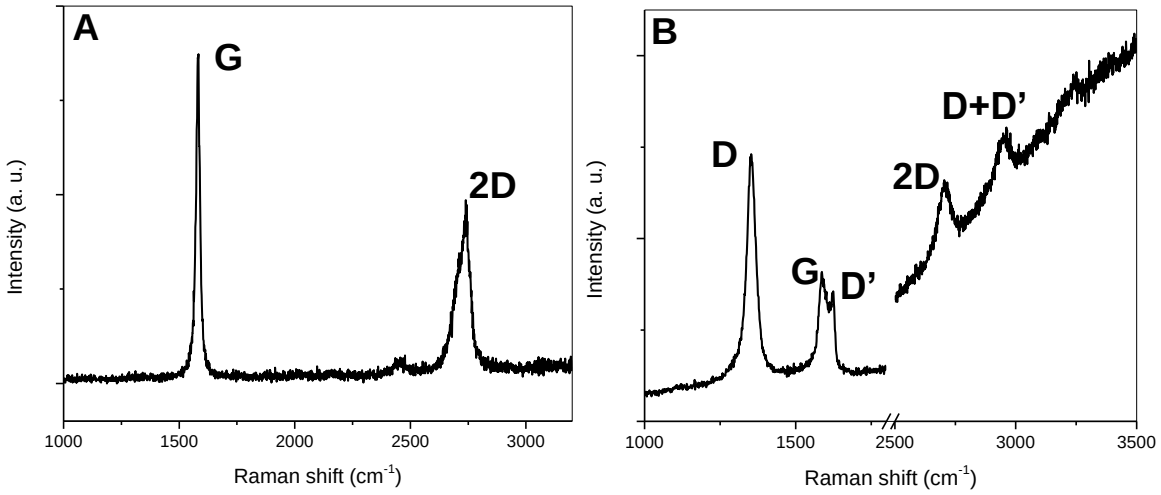

FIG. 1. *Typical Raman spectrum (at 488 nm) of FLG; (**A**) before and (**B**) after exposure to the hot-filament-promoted hydrogenation process.*

For FLG, in comparison with monolayer graphene (1LG), the 2D to G peak relative intensity ratio is lower (below 1) and the full width at half maximum (FWHM) of the 2D peak is higher [77]. Following the hydrogenation process, significant changes in the spectra can be observed (FIG. 1B). A narrow D peak of high relative intensity, higher than the G peak, dominates the spectra. The D' and D+D' peaks of lower relative intensity are also observed. Such spectra are obtained on material supported by the copper grid or on the material suspended on top of the grid holes. Those changes in Raman spectra have been previously reported for partially hydrogenated graphene [19]. The D, D' and D+D' peaks are activated by defects, which could be vacancies, edge defects, or C-H binding [19]. In the case of 1LG, it was shown that the relative intensity of D and D', or the ratio of their height, can be used to determine the type of defects [78]. The ratio of the height of the D and D' peaks, $h_D/h_{D'}$, is found to be lower than 2.7. In the case of the spectrum shown in FIG. 1B, this ratio is of 2.63. This ratio cannot be used here to determine the type of defects as FLG are concerned instead of 1LG. However the ratio of the height of the D and G peaks, h_D/h_G, is 2.13, which is

comparable to data previously published for hydrogenated 1LG and 2LG [19]. Assuming that the layers below the surface layers, which contribute to the G peak intensity, do not contribute to the D peak because defects are created at the surface in the absence of ions in the process, this h_D/h_G indicates a high content of defects on surfaces, which could be C-H bonding.

A region characterized by the spectrum shown on FIG. 1B was purposely exposed to longer laser irradiation time in order to induce a possible change in the structure such as hydrogen exodiffusion in case defects would be C-H bonding (laser power on the sample below 1 mW; exposure time of 60 s). FIG. 2 shows the spectrum, taken at 488 nm, obtained after such treatment.

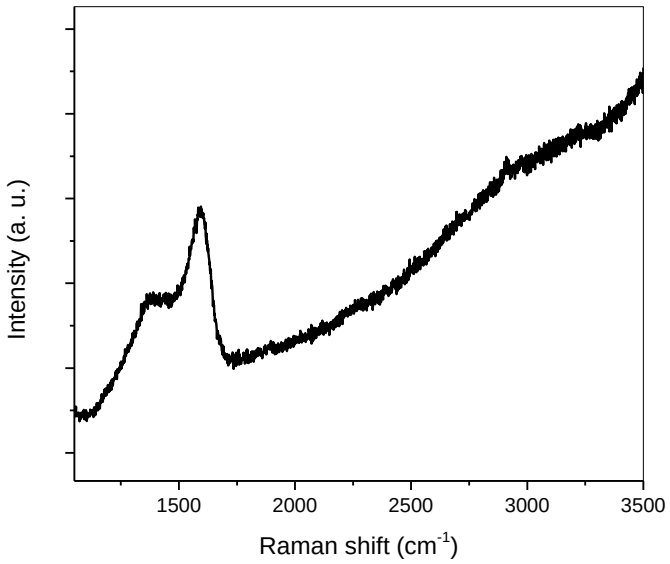

FIG. 2. *Typical Raman spectrum (at 488 nm) of FLG exposed to the hot-filament-promoted hydrogenation process and then to long time laser irradiation during Raman spectroscopy analysis (see text).*

There is a drastic change in the spectrum as compared to the spectrum obtained after a shorter laser exposure (FIG. 1B). The spectrum is composed of a wide band between 1100 and 1750 cm^{-1}, which includes the D and G bands. The 2D and D+D' bands are no longer observed as in FIG. 1B. This wide band between 1100 and 1750 cm^{-1} is typical of hydrogenated amorphous carbon (a-C:H) [30,79,80,81] (hydrogen content typically between 20 and 37 at.% [81]). This result strongly indicates that defects generated in FLG upon H exposure are C-H bonding. Hence it is supposed that hydrogenated FLG are converted into a-C:H under longer laser exposure. This result is consistent with the baseline observed in FIGs 1B and 2 which is likely to be related to the well-known luminescence effect due to CH groups [30,82].

FIG. 3 displays other typical spectra, taken at 514.5 nm, of the same sample. There is no G peak nor 2D peak from FLG. However, in the 1000-1800 cm^{-1} Raman shift region (FIG. 3A-C), the spectrum shows two peaks of low relative intensity on a strong luminescence background: a wide peak centered at ~1360 cm^{-1} (FIG. 3C) which is interpreted as the D peak from disordered sp^2-C arrangements [83], and a sharp peak centered at ~1060 cm^{-1} (FWHM of 8 cm^{-1}) (FIG. 3B) which is interpreted as the T peak from sp^3-C-C, previously reported as a wide and low relative intensity band in UV Raman spectra of ta-C [84,85]. A high intensity and narrow peak in the visible Raman spectra of transpolyacetylene has been reported at the same position but it is always associated to another band at 1450 cm^{-1} [86]. Likewise, a high intensity and narrow peak at 1090 cm^{-1} was detected in visible Raman spectra of diamond clusters of about 5 nm in diameter, which have been shown to be free of graphite-like sp^2 bonded structures [87]. Since electron energy loss spectroscopy studies showed strong surface plasmon, it was hypothesized that this mode was due to surface plasmon. However this assumption was not confirmed by observing whether the peak moves to lower frequencies as the dielectric constant of the surrounding medium increases, and that it grows in intensity as the crystalline size decreases. Taking into account that, for visible energies, the Raman scattering of sp^2-carbon is a resonant process about 50 to 230 times more effective than that of sp^3-carbon [65], both the absence of high relative intensity sp^2-C related features in visible Raman spectra and the presence of a sharp T peak indicate the conversion of sp^2-carbon into sp^3-carbon. This will be further discussed below. In the 2600-3200 cm^{-1} Raman shift region, the spectrum displays two bands with low relative intensities, centered at ~2853 and ~2940 cm^{-1} respectively. The first band was predicted for diamane [7] while the second one is interpreted as the C-H band [85,88], which is consistent with the strong luminescence background (FIG. 3).

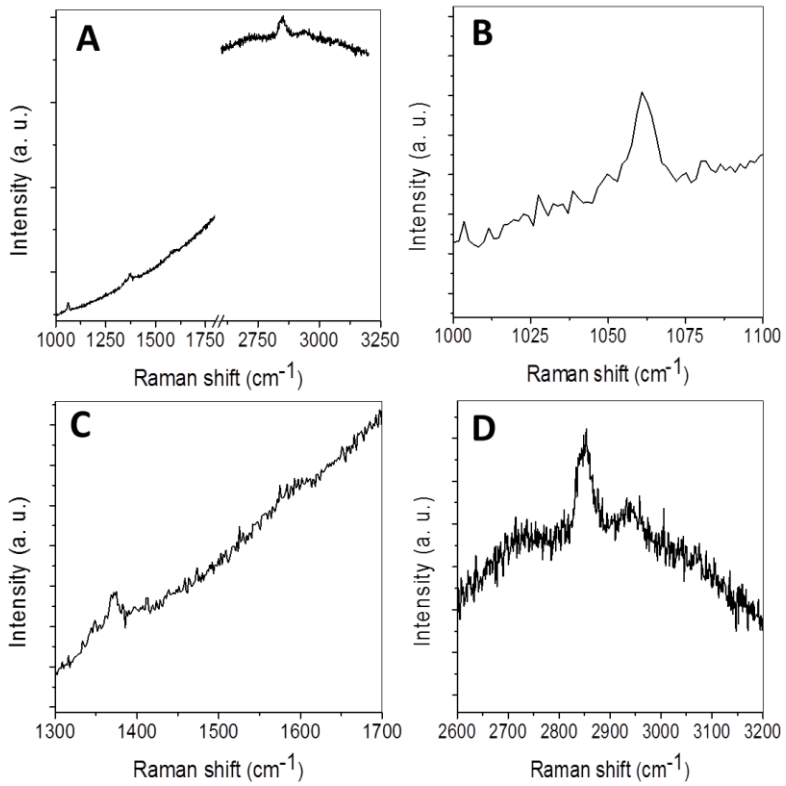

FIG. 3. *Typical visible Raman spectra of FLG exposed to the hot-filament-promoted hydrogenation process (at 514.5 nm); (**A**) full spectrum between 1000 and 3250 cm^{-1}; (**B**) zoom of the T peak spectral region; (**C**) zoom of the 1300-1700 cm^{-1} spectral region; (**D**) zoom of the 2600-3200 cm^{-1} spectral region.*

In some region of the same sample, additionally to the T and G peaks, two others peaks centered at ~1290 and ~1317 cm^{-1} are observed (FIG. 4). Those peaks have been previously ascribed to lonsdaleite in both experimental [89,90,91] and calculation works [7,92].

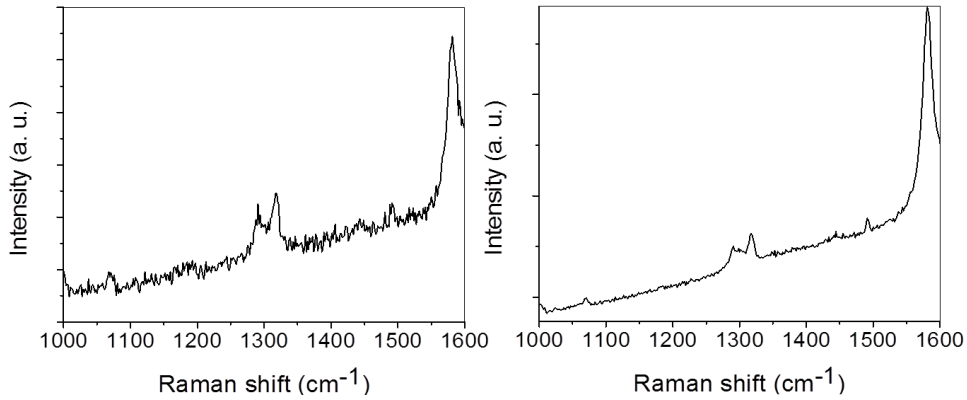

FIG. 4. *Typical visible Raman spectra of FLG exposed to the hot-filament-promoted hydrogenation process (at 514.5 nm).*

The features shown in visible Raman spectra shown in FIGs. 3 and 4 are further evidences of the formation of C-H bonds and other structural transformation of FLG as further discussed below.

3.2. FTIR microscopy

To directly detect C-H bonding, FTIR mapping was carried out. FIG. 5A shows a FTIR-ATR image processed on the integrated intensity of C-H stretching band. The image was obtained on the plain part of the TEM grid which circles the grid mesh, and which was exposed to H radicals. Prior treatment, this region of the grid contains FLG as evidenced by Raman spectroscopy analysis (FIG. 1A). FIG. 5A reveals a large-sized circular area of ~150 μm^2 containing C-H bonding, which first confirms that defects generated during the hydrogenation process are indeed C-H bonding and, second, indicates that hydrogenation took place in the basal plane of graphene, not only at the edges of graphene domains. FIG. 5B displays one absorbance spectra taken in the region identified by a white arrow in FIG. 5A.

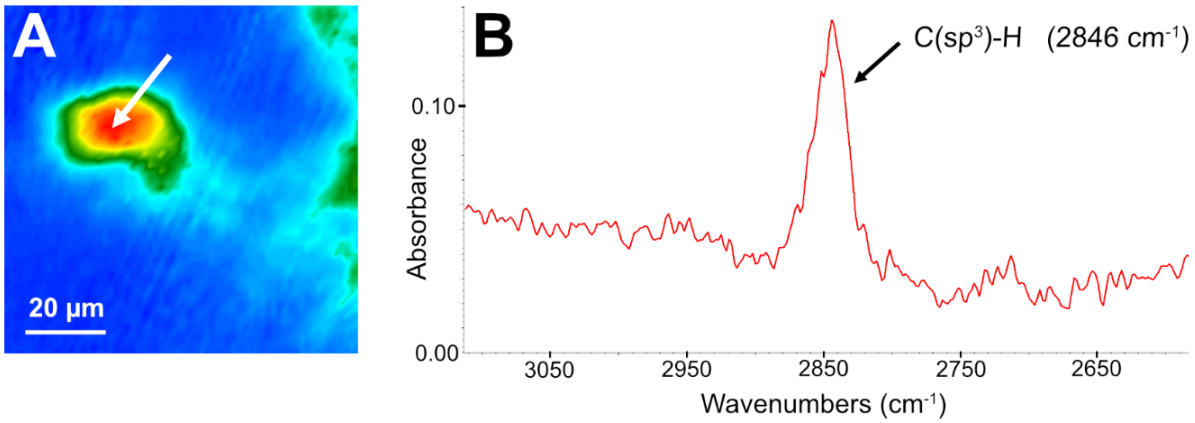

FIG. 5. *(**A**) Typical FTIR-ATR microscopy image processed on the integrated intensity of C-H stretching band of FLG exposed to the hot-filament-promoted hydrogenation process; (**B**) Typical absorbance FTIR spectrum (cumulated over 5 spectra) taken in the region arrowed in (**A**).*

FIG. 5B shows that the narrow C-H stretching band, which is centered at around 2846 cm^{-1}, is composed of only one among the nine possible vibration mode components. It is proposed that this mode corresponds to the C(sp^3)-H stretching mode. This assignment is based on the following arguments:

1. Taking into account vibration modes in free molecules [93], within the wavenumber range of 2800 to 2900 cm^{-1}, it is expected to detect the following vibration modes: C(sp^3)-H centered at ~2900 cm^{-1}, C(sp^3)-H_2 symmetrical centered at ~2875 cm^{-1} and C(sp^3)-H_3 symmetrical centered at ~2850 cm^{-1}. However, although the infrared (IR) absorption cross-section of the C-H stretching vibration modes is unknown in hydrogenated FLG and in ultrathin and crystalline sp^3-bonded carbon sheets, it is expected that the C(sp^3)-H_2 symmetrical and C(sp^3)-H_3 symmetrical modes would be simultaneously detected with their antisymmetrical counterpart, which is not the case since the observed C-H stretching band is composed of only one vibration mode component. Therefore, the C(sp^3)-H_2 symmetrical and C(sp^3)-H_3 symmetrical modes are excluded.

2. The C(sp^2)-H olefinic and C(sp^2)-H aromatic modes are not considered as they are typically detected at much higher wavenumber, above 2975 cm^{-1} in the case of free molecules [93].

3. The C_2H_2 olefinic symmetrical and antisymmetrical modes are also typically detected at significantly higher wavenumber, above 2950 cm^{-1}, in the case of free molecules [93]. Furthermore, they would be accompanied by their anti/symmetrical counterpart, which is not the case here, since the observed C-H stretching band is composed of only one vibration mode component.

4. Our experimental value is consistent with calculated C-H stretching mode frequency for graphane, 2H-(AB)D, (AB)D, and 2H-(ABC)D (TAB. 1). The C-H stretching mode frequencies of isolated H on graphene and on single vacancy in graphene are found to be much higher giving a further evidence of high hydrogenation degree. Only the C-H stretching mode frequency of AB stacking in 2H-(AB)D and ABC stacking in 2H-(ABC)D were calculated as we found that AB stacking is more stable than AA stacking, and that ABC stacking is more stable than AAA and ABB stacking.

Structure	**Frequency (cm^{-1})**
Isolated H on Graphene	3670
Isolated H on Single Vacancy in Graphene	3210
Graphane	2890
2H-(AB)D	2880
2H-(ABC)D	2890

TAB. 1. *Calculated C-H stretching mode frequency in various structures.*

The detection of the C(sp^3)-H stretching mode is a remarkable result since the IR absorption cross-section for this mode is expected to be significantly lower than the values for the other modes, as in

free molecules [93]. In free molecules, the IR absorption cross-section for the C(sp^3)-H stretching mode is between 18.6 and 31.6 times lower than the corresponding value for C(sp^3)-H_3 and C(sp^3)-H_2 stretching modes [93]. The shift, by around 54 cm^{-1}, of the position of the C(sp^3)-H mode peak, as compared to the corresponding position in free molecules [93], is theorized to result from the structure change generated by the hydrogenation of FLG, the subsequent conversion of sp^2 hybridization into sp^3 hybridization, and the interlayer sp^3-C bond formation as further discussed below.

The narrow, one component C-H stretching band reveals that carbon atoms are bonded to one hydrogen atom. This single component narrow C-H stretching band has never been reported before in the case of hydrogenated graphene. Known disclosures on FTIR spectroscopy analysis of hydrogenated graphene report on a wide multi-component C-H stretching band including C(sp^3)-H_3 and C(sp^3)-H_2 modes instead of C(sp^3)-H mode [27,39,41,42,43,44,45], consistent with graphene domains of reduced size which are hydrogenated only on their edges. Comparatively, the relatively intense one component narrow C-H stretching band shown here is representative of large-size (~150 μm^2) graphene hydrogenated on faces so that the related FTIR signal prevails over that generated by the hydrogenated graphene edges.

3.3. UV Raman spectroscopy

As pointed out in the Introduction section, in the visible, Raman scattering is much more effective in probing sp^2-carbon than sp^3-carbon. UV excitation is necessary to obtain a more evenly weighted probe of both types of hybridized-carbon and to avoid strong luminescence background. TAB. 2 provides the graphane, 2H-(AB)D and 2H-(ABC)D band-gap values from HSE and G_0W_0 approaches. The graphane values are in good agreement with previous studies [94,95,96]. This is the first report of 2H-(AB)D and 2H-(ABC)D fundamental band-gap from GW calculations. TAB. 2 justifies the use of a deep UV excitation for Raman spectroscopy study of ultrathin and crystalline C(sp^3) film. In the case of 2H-(ABC)D, according to the phonon dispersion curve at Γ-point (FIG 6), peaks are expected at the following frequencies: around 290, 480, 850, 1140, 1240, 1290, 1315 and 2890 cm^{-1}. As discussed above, two of those peaks, at 1290 and at 1317 cm^{-1}, were observed in visible Raman spectra (FIG. 4).

Band-Gap in Γ (eV)	Graphane	2H-(AB)D	2H-(ABC)D
HSE	4.4	3.9	3.6
G_0W_0	5.8	4.8	4.3

TAB. 2. *Calculated graphane, 2H-(AB)D and 2H-(ABC)D fundamental band-gaps values from HSE and G_0W_0 approaches.*

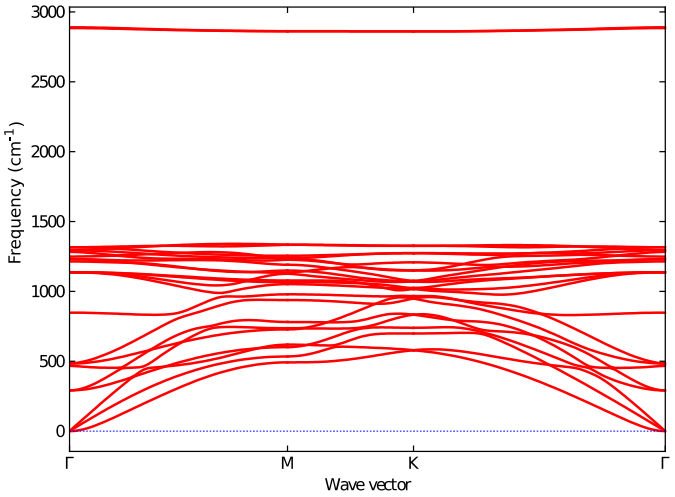

FIG. 6. *Phonon dispersion curve of 2H-(ABC)D.*

FIGs. 7B-E show representative UV Raman spectra of FLG exposed to H radicals. No difference was evidenced whether the spectra are obtained in the vicinity of the copper-supported region of the TEM grid analyzed by FTIR microscopy (FIG. 5) or in the TEM grid mesh where free-standing FLG are originally located. The spectra shown in FIGs. 7B-E are different from the spectra obtained before the hydrogenation process (FIG. 7A).

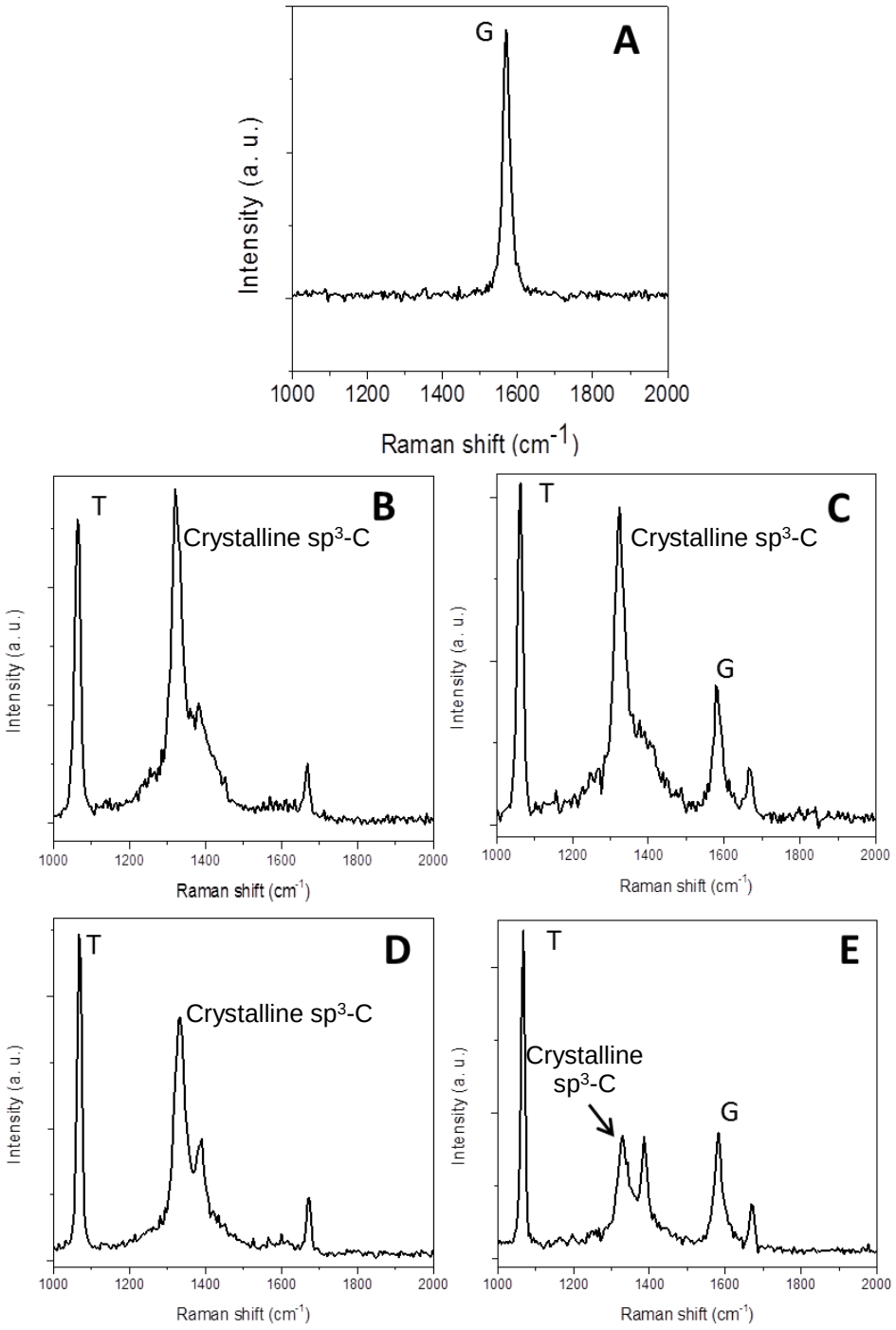

FIG. 7. *Typical UV Raman spectra of FLG (**A**) before and (**B-E**) after the exposure to the hot-filament-promoted hydrogenation process (at 244 nm).*

The spectrum shown in FIG. 7B displays two sharp peaks centered at ~1063.0 and ~1323.1 cm^{-1}, respectively. The FWHM of those two peaks is of ~15.6 and 30.2 cm^{-1}, respectively. The first peak is interpreted as the *T* peak, due to C-C sp^3 vibration, found in ta-C films as a low-intensity and

broad band [84,85] or as a high-intensity and narrow peak in diamond nanoclusters [87] and which was detected under visible excitation as shown above (FIGs. 3A and 3B). The peak centered at ~1323.1 cm^{-1} could be interpreted as corresponding to two vibrational modes of lonsdaleite [7,89,90,92] which were detected under visible excitation as shown above (FIGs. 4). Those modes are the A_{1g} and E_{2g} modes, corresponding to the triply-degenerate stretching mode of cubic diamond, which are, in lonsdaleite, split into a component vibrating in the plane of the layers and a component vibrating perpendicular to the layers [92]. Unlike graphite, the bonding strength of lonsdaleite is comparable whether it is parallel or perpendicular to the layers and the wavenumber separation between the A_{1g} and E_{2g} modes is expected to be small [92]. Alternatively, the peak could be interpreted as corresponding to the diamond peak [65] which would be shifted because of stress [48] or because of confinement effects in few atomic layers or in sub-10 nm nanocrystals [97,98]. Here, the *T* peak is narrow and of high relative intensity, indicating that the structure of the *C*(sp^3) in the material is crystalline, as opposed to the FWHM of the *T* peak in ta-C which is wide because of the amorphous structure. The C(sp^3) features in Raman spectra are consistent with the detection of only one component in the FTIR C-H stretching band as shown above (FIG. 5). Another example is provided as FIG.7C, with the *T* peak at 1061.6 cm^{-1} (FWHM of 17.3 cm^{-1}) and the diamond/lonsdaleite peak at 1323.5 cm^{-1} (FWHM of 30.9 cm^{-1}). Hence, the Raman spectroscopy results show that it is possible to form crystalline sp^3-carbon ultrathin sheets from the hydrogenation of FLG at low temperature and low pressure and the subsequent formation of interlayer C(sp^3) bonds. The relatively large FWHM value of the diamond/lonsdaleite peak may reveal confinement effects in few atomic layers or in sub-10 nm nanocrystals [97,98] or diamond/lonsdaleite hybrid structure. The laminar character of diamond/lonsdaleite will be further discussed below.

In most of the regions, the *T* and diamond/lonsdaleite peaks are simultaneously detected as shown in FIGs.7B to 7E and in FIG. 8. From the analysis of 329 spectra taken from four maps and three samples, variations in peak position are observed. The position of the T and diamond/lonsdaleite peaks is found to vary within a range of 16.4 cm^{-1} and 17.5 cm^{-1}, respectively and, more interestingly, both peak positions vary in parallel so that there is a clear correlation between them (FIGs. 8 and 9). In addition, the diamond/lonsdaleite peak is found to vary from 1319.5 to 1337 cm^{-1}, therefore including 1332 cm^{-1} which is the value for diamond [65]. However, those two results do not allow clearly identifying the actual structure, as they are consistent with the occurrence of both lonsdaleite and diamond as well as a variable combination of both. The C(sp^3) symmetry obtained upon hydrogenation and subsequent C(sp^2) to C(sp^3) transformation could

indeed depend primarily on the relative orientation of the superimposed graphenes in the primary FLG.

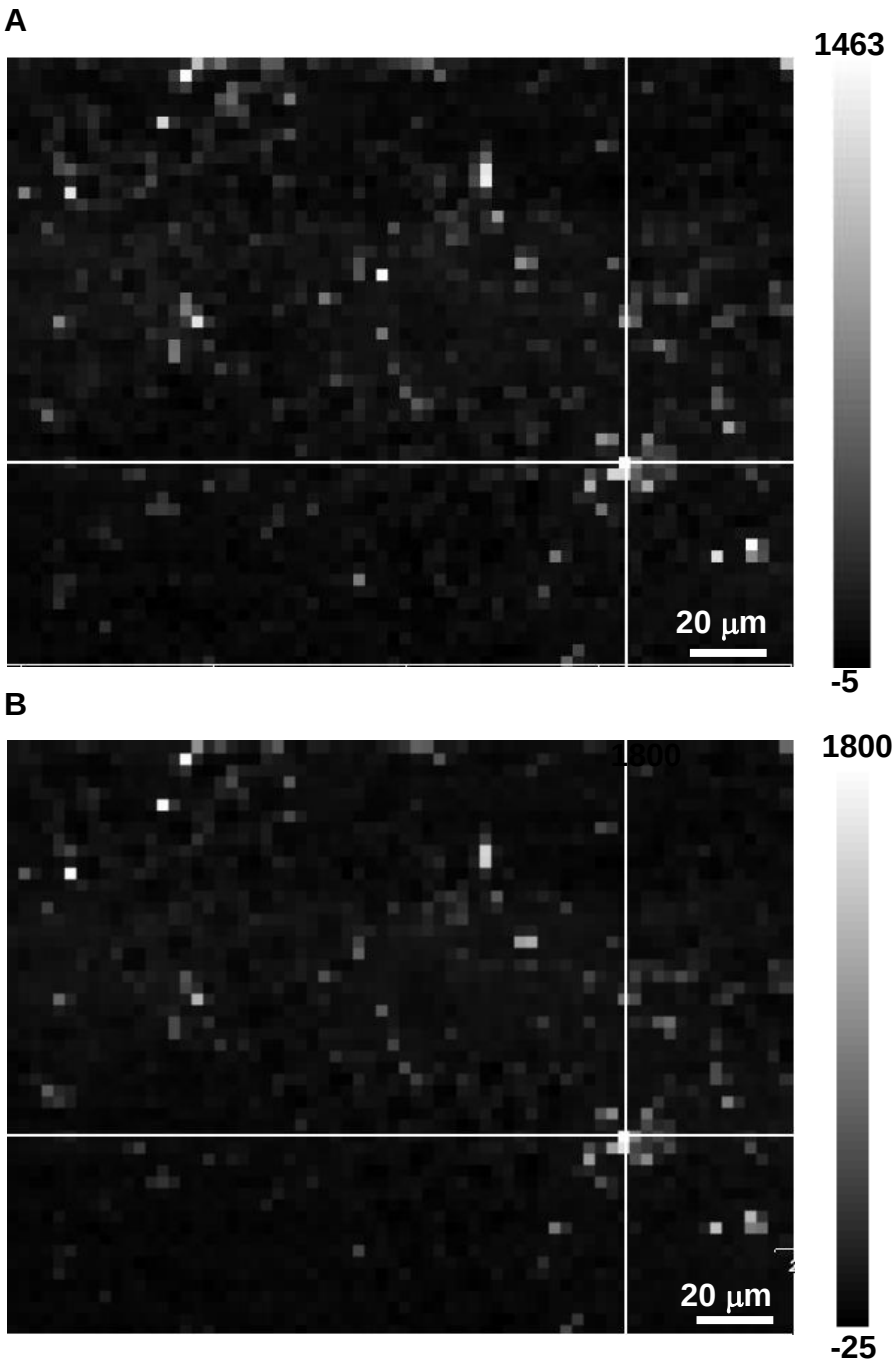

FIG. 8. *Comparison of UV Raman maps of (**A**) the intensity of the T peak with (**B**) the intensity of the diamond/lonsdaleite peak in the same region (at 244 nm).*

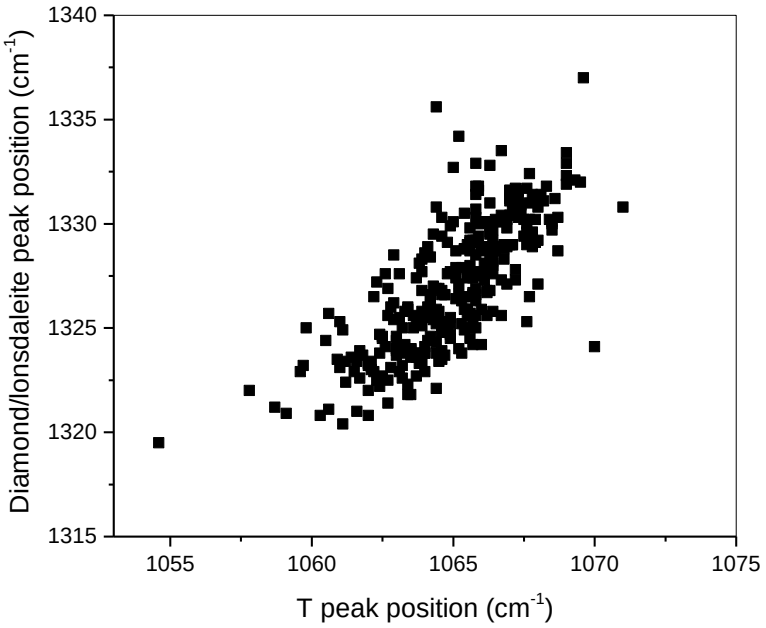

FIG. 9. *Diamond/lonsdaleite stretching mode Raman peak position as a function of the* T *peak position in FLG exposed to the hot-filament-promoted hydrogenation process (spectra taken at 244 nm).*

In some regions of the grid, the T peak and the lonsdaleite or diamond peak are simultaneously detected along with the graphene G peak at ~1582 cm^{-1} (FIGs. 7C and 7E, respectively). The relative intensity of both the lonsdaleite or diamond peak and that of the *G* peak varies depending on the region probed by the laser. In some cases, the intensity of the *G* peak is several time higher than that of the *T* and diamond/lonsdaleite peaks. Those observations along with FIG.9 suggest that it is possible to prepare graphene-lonsdaleite/diamond hybrids from the partial conversion of FLG into lonsdaleite, or diamond, or both. It is hypothesized that the variation of the relative intensity of the peaks related to C(sp^2) and C(sp^3) may be indicative of the sp^2/sp^3 ratio in the hybrid material. Also, the UV spectra (FIGs. 7B-E) show a peak at 1620 cm^{-1}, which was previously attributed to a particularly stable defect in diamond consisting of an isolated sp^2 bonded pair [99].

In order to verify the physical origin of the T peak, a region of 2LG exposed to the hot-filament promoted hydrogenation process where this peak was the only one detected was over-exposed to the UV laser in order to induce a possible structure transformation. In fact the measurement was repeated on the same spot under the same conditions (6 mW power at the entrance of the microscope; duration of 1 s). FIGs. 10A and 10B show the spectrum of that region after the

first and repeated measurements, respectively. After the second measurement, the G peak appears in the spectrum (FIG. 10B). This experiment confirms that the T peak is from C(sp^3)-C(sp^3).

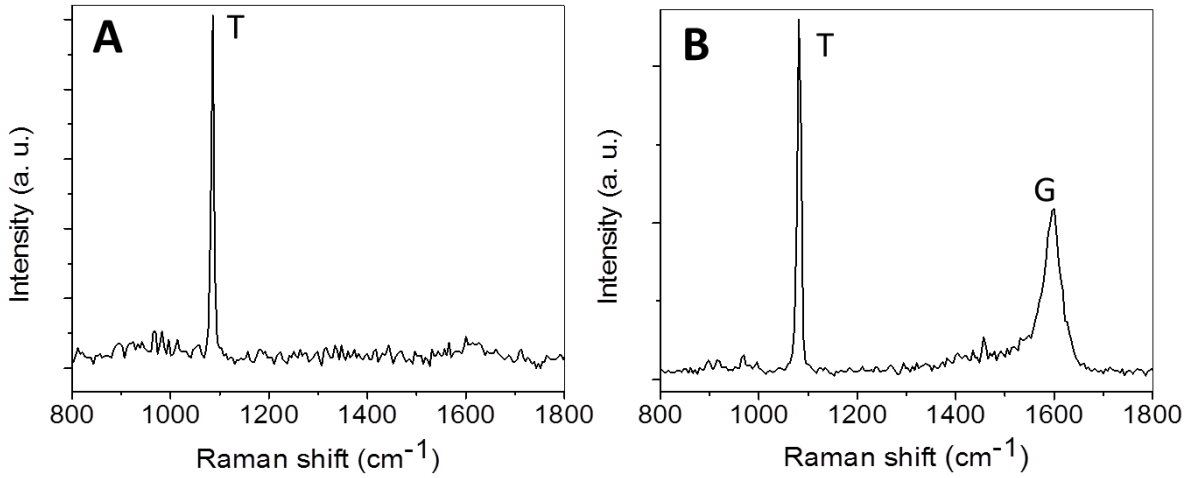

FIG. 10. *Typical Raman spectra (at 244 nm) of a 2LG film exposed to the hot-filament-promoted hydrogenation process after, (**A**) a first measurement and (**B**) a repeated measurement.*

FIG. 11 displays UV Raman maps of the intensity of diamond/lonsdaleite stretching mode Raman peak of FLG TEM grids exposed to the hot-filament-promoted hydrogenation process. FIG. 11A shows that diamond/lonsdaleite stretching mode Raman peak can be detected in multiples regions in a surface area of ~220x140 μm^2. FIG. 11B and FIG. 11C show some examples of extended regions of ~33x51 μm^2 (FIG. 11B), ~21x33 μm^2 (FIG. 11C) and ~15x15 μm^2 (FIG. 11C), where lonsdaleite or diamane or diamond are continuously detected. These dimensions are consistent with that of the hydrogenated region revealed by FTIR microscopy (FIG. 5).

Although electron microscopy analyses would help confirming this hypothesis, the fact that C(sp^3)-H_3 and C(sp^3)-H_2 vibration modes that should be detected in hydrogenated crystalline sp^3 clusters, were not detected in FTIR spectra although their IR absorption cross-section are expected to be significantly higher than the values for the C(sp^3)-H mode, as in free molecules [93], strongly suggest that part of the laminar character of the material has been conserved upon sp^2 to sp^3 conversion.

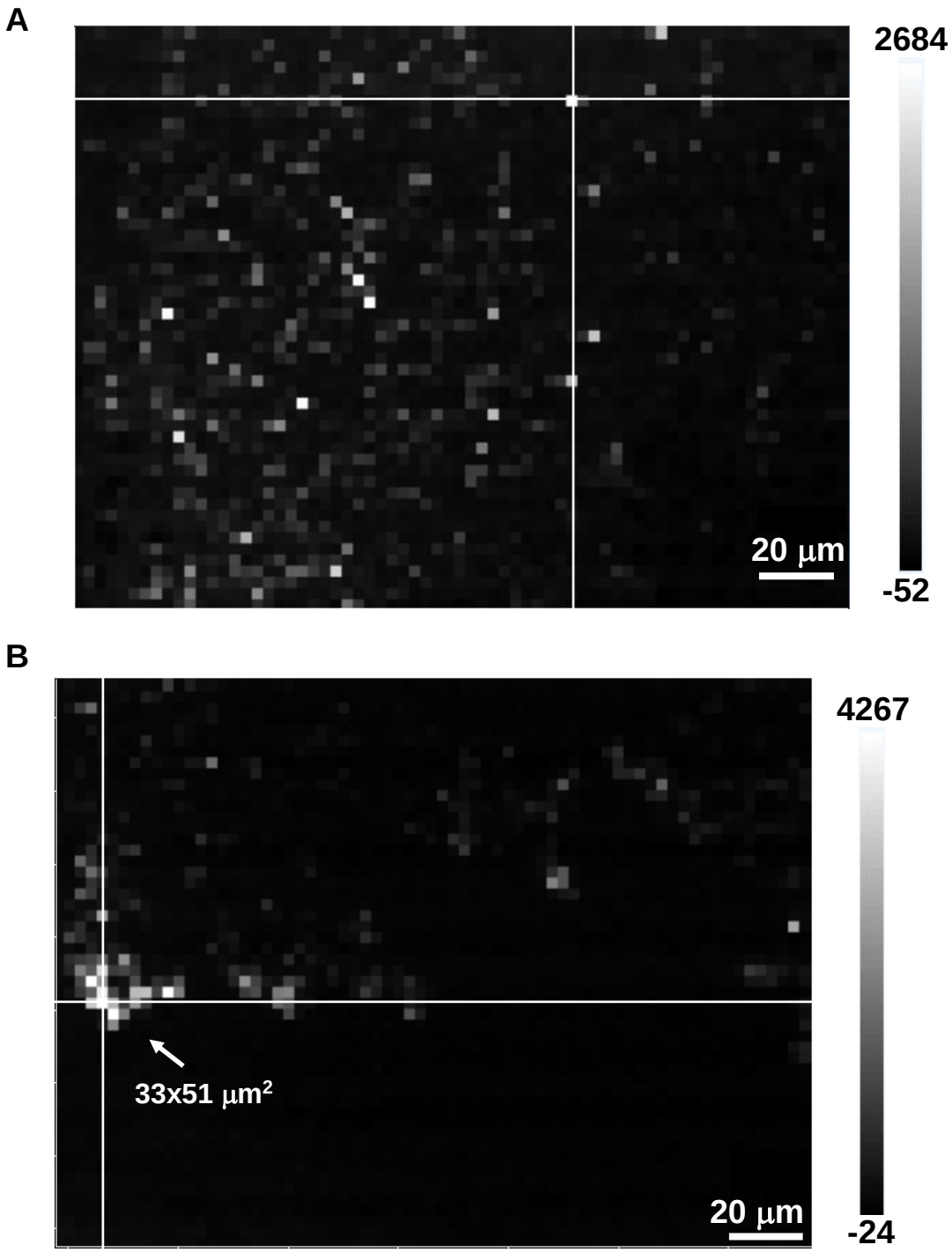
A
2684
20 μm
-52
B
4267
33x51 μm²
20 μm
-24

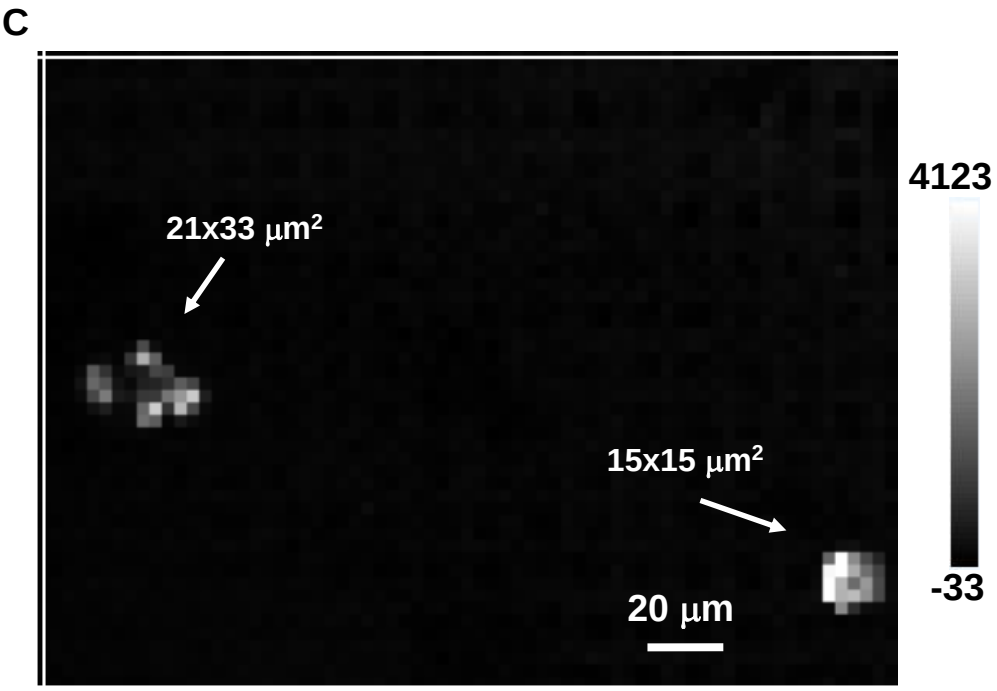

FIG. 11. *Typical UV Raman maps of the intensity of the* diamond/lonsdaleite stretching mode Raman *peak of FLG exposed to the hot-filament-promoted hydrogenation process (at 244 nm).*

The possibility of producing few-layer crystalline sp^3-bonded carbon at low temperature and at low pressure, by the exposure of FLG to the hot-filament-promoted hydrogenation process is of great technological interest for a wide range of applications (see section 1) [100]. Our results have also wider scientific implications. For instance, they may help at clarifying the origin and formation mechanism(s) of meteoritic and interstellar diamond dust grains, including those supposed to be presolar [101]. As reviewed in Ref [102], "*Opinions regarding the formation mechanism(s) of meteoritic and interstellar diamond grains have changed over the years as new methods of making synthetic diamond were developed…*". Our results could reveal the existence of an additional formation route of diamond grains wherein FLG grains are converted into lonsdaleite, diamond or other polytypes by exposure to H flux without requiring high pressure. Those conditions can actually exist in space, for instance in the circumstellar envelope of C-rich evolved stars. And then, there are clues for the needed pre-existence of FLG in space: the possible extragalactic detection of planar C_{24} was reported by using the *Spitzer* Space Telescope although it has not yet been confirmed through laboratory infrared spectroscopy at different temperatures, which is extremely difficult

because of the high reactivity of C_{24} [103]; also, recently, it has been speculated from laboratory experiments that FLG grains could be formed in space from pyrene [104].

5. Conclusion

Thanks to combined Raman spectroscopy and FTIR microscopy investigations, the possibility of obtaining various crystalline C(sp^3) structures (diamond and/or lonsdaleite and/or diamane and/or hybrids of those) from a C(sp^2) structure (few-layer graphene film) at low temperature and low pressure was demonstrated, by means of a hydrogenation process. This statement is reasonably ascertained from mostly two unprecedented observations: (i) The combined occurrence of both a sharp so-called *T* peak (at ~1055-1071 cm^{-1}, assigned to C(sp^3)-C(sp^3) bonds) and a diamond/lonsdaleite stretching mode Raman peak (at 1319-1337 cm^{-1}, usually assigned to lonsdaleite or diamond) as evidenced by Raman over sample surfaces as large as 1,683 μm^2; (ii) the occurrence of a single vibration mode in the C-H stretching band, hence assigned to the prevalent presence of C(sp^3)-H groups over any other group involving more than one H, over sample surfaces as large as 150 μm^2.

More in the details, the work also brought a couple of other new experimental observations and findings: (i) a 54 cm^{-1} shift of the C(sp^3)-H mode as compared to the case of free molecules is observed, as a consequence of the sp^2-to-sp^3 conversion upon hydrogenation and subsequent difference in resulting atomic environment with respect to small, isolated molecules; (ii) in addition to the formation of isolated crystalline and ultrathin sp^3-carbon sheets over surfaces as large as 33x51 μm^2, the combined signals of graphene and crystalline and ultrathin sp^3-carbon sheets are also observed, suggesting the formation of crystalline and ultrathin sp^3-carbon sheets /graphene hybrid materials. Further studies are however needed to ascertain in which extent the film morphology was maintained; (iii) the sp^2-to-sp^3 transformation and resulting structure (diamond, or lonsdaleite, or hybrid) is assumed to depend on the number of graphenes in the former FLG and the relative orientation of the stacked layers.

Finally, the work presented here makes a significant technological advance by introducing the hot filament process for the efficient production of atomic hydrogen from gaseous H_2, applied to the efficient hydrogenation of FLG and the subsequent formation of crystalline and ultrathin sp^3-carbon sheets as a new route for the C(sp^2)-to-C(sp^3) allotropic transformation. It also makes a

significant scientific advance by providing a new clue for understanding the origin of sp^3 carbon structures in specific (e.g., extraterrestrial) environments.

Acknowledgements

This research was funded by the Ministry of Higher Education, Science and Technology of the Dominican Republic (2010-2011, 2012 and 2015 FONDOCyT programs). F.P. and M.M. greatly acknowledge MESCyT and PUCMM for strong financial, administrative and technical support; 2017 NEXT Guest scientist Program (www.next-toulouse.eu/guest-scientists) and the French Embassy in the Dominican Republic for travel support. F.P. is thankful to Richard Bormett from Renishaw for technical support with Raman spectroscope. I.C.G. acknowledges the *Calcul en Midi-Pyrénées* initiative, CALMIP (Project p0812), for computer time allocation. This work was also granted access to the HPC resources of CINES and IDRIS under the allocation 2018-A0040906649 made by GENCI.

References

[1] Chernozatonskii LA, Sorokin PB, Kvashnin A, Kvashnin DG. Diamond-Like C_2H Nanolayer, Diamane: Simulation of the Structure and Properties, J Exp Theor Phys Lett 2009;90:134-138.

[2] Leenaerts O, Partoens B, Peeters FM. Hydrogenation of bilayer graphene and the formation of bilayer graphane from first principles. Phys Rev B 2009; 80:245422-1-245422-6.

[3] Zhu L, Hu H, Chen Q, Wang S, Wang J, Ding F. Formation and electronic properties of hydrogenated few layer graphene. Nanotechnology 2001;22:185202.

[4] Chernozatonskii LA, Sorokin PB, Kuzubov AA, Sorokin BP, Kvashnin AG, Kvashnin DG et al. Influence of Size Effect on the Electronic and Elastic Properties of Diamond Films with Nanometer Thickness. J. Phys. Chem. C 2011;115:132-136.

[5] Barboza A.P.M., Guimaraes M.H.D., Massote DVP, Campos LC, Barbosa Neto NM, Cancado LG et al. Room temperature compression-induced diamondization of few-layer graphene. Adv. Mater. 2011;23:3014-3017.

[6] Li LS, Zhao X. Transformation between different hybridized bonding structures in two-dimensional diamond based materials. J Phys Chem C 2011;115:22168-22179.

[7] Chernozatonskii LA, Mavrin BN, Sorokin PB. Determination of ultrathin diamond films by Raman spectroscopy. Phys Status Solidi B 2012; 249:1550-1554.

[8] Muniz AR, Maroudas D, Opening and tuning of band gap by the formation of diamond superlattices in twisted bilayer graphene. Phys Rev B 2012;86:075404-1-075404-11.

[9] Li H, Li J, Wang Z, Zou G. Layer number-dependant structural evolution of two-dimensional diamond films. Chem Phys Lett 2012;550:130-133.

[10] Ruoff RS. Personal perspectives on graphene: New graphene-related materials on the horizon. MRS Bulletin 2012;37:1314-1318.

[11] Odkhuu D, Sin D, Ruoff RS, Park N. Conversion of multilayer graphene into continuous ultrathin sp^3-bonded carbon films on metal surfaces 2013. Scientific Reports 3:3276-1-3276-7; DOI: 10.1038/srep03276.

[12] Rajasekaran S, Abild-Pedersen F., Ogasawara H., Nilsson A., Kaya S. Interlayer carbon bond formation induced by hydrogen adsorption in few-layer supported graphene. Phys Rev Lett 2013; 111: 085503-1-0585035.

[13] Machado AS, Maroudas D, Muniz AR. Tunable mechanical properties of diamond superlattices generated by interlayer bonding in twisted bilayer graphene. Appl Phys Lett 2013;103: 013113-1013113-5.

[14] Kvashnin AG, Chernozatonskii LA, Yakobson BI, Sorokin PB. Phase diagram of quasi-two dimensional carbon, from graphene to diamond. Nano Letters 2014;14:676-681.

[15] Martins LGP, Matos MJS, Paschoal AR, Freire PTC, Andrade NF, Aguiar AL, Kong J, Neves BRA, de Oliveira AB, Mazzoni MSC, Filho AGS, Cancado LG. Raman evidence for pressure-induced formation of diamondene, Nat. Comm. 2017;8 (1) 96 (9 pages).

[16] Gao Y, Cao T, Cellini F, Berger C, de Heer WA, Tosatii E, Riedo Elisa, Bongiorno A. Ultrahard carbon film from epitaxial two-layer graphene, Nature Nanotechnology 2018;13:133-138.

[17] Bianco A, Chen Y, Chen Y, Ghoshal D, Hurt RH, Kim YA, Koratkar N, Meunier V, Terrones M. A carbon science perspective in 2018: Current achievements and future challenges. Carbon 2018;132:785-801.

[18] Ruoff RS. A perspective on objectives for carbon science. Carbon 2018;132:802.

[19] Elias DC, Nair RR, Mohiuddin TMG, Morozov SV, Blake P, Halsall MP et al. Control of graphene's properties by reversible hydrogenation: evidence for graphane. Science 2009; 323: 610-613.

[20] Sofo JO, Chaudhari AS, Barber GD. Graphane: A two-dimensional hydrocarbon. Phys Rev B 2007;75:153401-1-153401-4.

[21] Nair RR, Ren W, Jalil R, Riaz I, Kravets VG, Britnell L et al. Fluorographene: A Two-Dimensional Counterpart of Teflon. Small 2010;6(24):2877-2884.

[22] Touhara H, Kadono K, Fujii Y, Watanabe N. On the structure of Graphite Fluoride. Z Anorg Allgem Chem 1987; 544:7-20.

[23] Pan Z, Sun H, Zhang Y, Chen C. Harder than Diamond : Superior Indentation Strength of Wurzite BN and Lonsdaleite. Phys Rev Lett 2009;102:055503-1-055503-4.

[24] Németh P, Garvie LAJ, Aoki T, Dubrovinskaia N, Dubrovinski L, Buseck PR. Lonsdaleite is faulted and twinned cubic diamond and does not exist as a discret material. Nature Comm. 2014;5(5447):1-5.

[25] Lin QY, Li TQ, Liu ZJ, Song Y, He LL, Hu ZJ, Guo QG, Ye HQ. High-resolution TEM observations of isolated rhombohedral crystallites in graphite blocks. Carbon 2012;50(6):2369-2371.

[26] Luo Z, Yu T., Kim K, Ni Z, You Y, Lim S et al. Thickness-dependent reversible hydrogenation of graphene layers. ACS Nano 2009;7: 1781-1788.

[27] Zheng L, Li Z, Bourdo S, Watanabe F, Ryerson CC, Biris AS. Catalytic hydrogenation of graphene films. Chem Commun 2011;47:1213-1215.

[28] Diankov G, Neumann M, Goldhaber-Gordon D. Extreme Monolayer-Selectivity of Hydrogen-Plasma reactions with Graphene. ACS Nano 2013;7:1324-1332

[29] Felten A, Eckmann A, Pireaux JJ, Krupke R, Casiraghi C. Controlled modification of mono- and bilayer graphene in O_2, H_2 and CF_4 plasmas. Nanotechnology 2013;24:355705.

[30] Robertson J. Diamond-like amorphous carbon. Mater Sci Eng R 2002; 37:129-281.

[31] Piazza F. Hard-hydrogenated tetrahedral amorphous carbon films by distributed electron cyclotron resonance plasma. Int J Refract Met Hard Mater 2006;24:39-48.

[32] Ryu S, Han MY, Maultzsch J, Heinz TF, Kim P, Steigerwald ML et al. Reversible basal plane hydrogenation of graphene. Nano Lett 2008;8(12):4597-602.

[33] Balog R, Jørgensen B, Wells J, Lægsgaard E, Hofmann P, Besenbacher F et al. Atomic Hydrogen Adsorbate Structures on Graphene. J Am Chem Soc 2009;131:8744-8745.

[34] Guisinger NP, Rutter GM, Crain JN, First PN, Stroscio JA. Exposure of Epitaxial Graphene on SiC(0001) to Atomic Hydrogen. Nano Lett 2009;9:1462-1466.

[35] Wang Y, Xu X, Lu J, Lin M, Bao Q, Özyilmaz B et al. Toward High Throughput Interconvertible Graphane-to-Graphene Growth and Patterning. ACS Nano 2010;4:6146-6152.

[36] Jones JD, Hoffmann WD, Jesseph AV, Morris CJ, Verbeck GF, Perez JM. On the mechanism for plasma hydrogenation of graphene. Appl Phys Lett 2010;97:233104-1-233104-3.

[37] Burgess JS, Matis BR, Robinson JT, Bulat FA, Perkins FK, Houston BH et al. Tuning the electronic properties of graphene by hydrogenation in a plasma enhanced chemical vapour deposition reactor. Carbon 2011;49:4420-4426.

[38] Wojtaszek M, Tombros N, Caretta A,.van Loosdrecht PHM,van Wees BJ. A road to hydrogenating graphene by a reactive ion etching plasma. J Appl Phys 2011;110:063715-1-063715-6.

[39] Poh HL, Sanek F, Sofer Z, Pumera M. High-pressure hydrogenation of graphene:towards graphane. Nanoscale 2012;4:7006-7011.

[40] Kataria S, Patsha A, Dhara S, Tyagi AK, Barshilia HC. Raman imaging on high quality graphene grown by hot-filament chemical vapor deposition. J. Raman Spectrosc 2012;43:1864–1867.

[41] Subrahmanyam KS, Kumar P, Maitra U, Govindaraj A, Hembram KPSS, Waghmare UV et al. Chemical storage of hydrogen in few-layer graphene. PNAS 2011;108:2674-2677.

[42] Yang Z, Sun Y, Alemany LB, Narayanan TN, Billups WE. Birch Reduction of Graphite. Edge and Interior Functionalization by Hydrogen. J Am Chem Soc 2012;134:18689-18694.

[43] Schäfer RA, Enlert JM, Wehrfritz P, Bauer W, Hauke F, Seyller T et al. On the Way to Graphane-Pronounced Fluoresence of Polyhydrogenated Graphene. Angew. Chem. Int. Ed. 2013;52:754-757.

[44] Krishna R, Titus E, Costa LC, Menezes JCJMDS, Correia MRP, Pinto S et al. Facile synthesis of hydrogenated reduced Graphene oxide via hydrogen spillover mechanism. J Mater Chem 2012;22:10457-10459.

[45] Sofer Z, Jankovsky O, Simek P, Soferova L, Sedmidubsky D, Pumera M. Highly hydrogenated graphene via active hydrogen reduction of graphene oxide in the aqueous phase at room temperature. Nanoscale 2014;6:2153-2160.

[46] Whitener Jr. KE, Lee WK, Campbell PM, Robinson JT, Sheehan PE. Chemical hydrogenation of single-layer graphene enables completely reversible removal of electrical conductivity, Carbon 2014;348:72-353.

[47] Pumera M, Wong CHA. Graphane and hydrogenated graphene. Chem Soc Rev 2013;42:5987-5995.

[48] Prelas MA, Popovici G, Bigelow LK. Handbook of Industrial Diamonds and Diamond Films. New York: Marcel Dekker; 1998.

[49] Butler JE, Sumant AV. The CVD of Nanodiamond Materials. Chem Vap Deposition 2008; 14:145-160.

[50] Zimmer J, Ravi KV, Aspects of scaling CVD diamond reactors. Diamond Relat Mater 2006;15: 229-233.

[51] Frenklach M, Wang H. Detailed surface and gas-phase chemical kinetics of diamond deposition. Phys Rev B 1991;43: 1520-1545.

[52] Stiegler J, Lang T, Von Kaenel Y, Michler J, Blank E. Activation energy for diamond growth from the carbon-hydrogen gas system at low temperatures. Appl Phys Lett 1997;70:173-175.

[53] Redman SA, Chung C, Ashfold MNR. H atom production on a hot filament chemical vapour deposition reactor. Diamond Relat Mater 1999;8:1383-1387.

[54] Redman SA, Chung C, Rosser KN, Ashfold MNR. Resonance enhanced multiphoton ionisation probing of H atoms in a hot filament chemical vapour deposition reactor. Phys. Chem Chem Phys 1999;1:1415-1424.

[55] Schäfer L, Klages CP, Meier U, Kohse-Höinghaus K. Atomic hydrogen concentration profiles at filaments used for chemical vapor deposition of diamond. Appl Phys Lett 1991;58:571-573.

[56] Chen KH, Chuang MC, Penney CM, Banholzer WF. Temperature and concentration distribution of H_2 and H atoms in hot-filament chemical-vapor deposition of diamond. J Appl Phys 1992;71(3):1485-1493.

[57] Connell LL, Fleming JW, Chu HN, Vesteck Jr DJ, Jensen E, Butler JE. Spatially resolved atomic hydrogen concentrations and molecular hydrogen temperature profiles in the chemical-vapor deposition of diamond. J Appl Phys 1995;78(6):3622-3634.

[58] Zumbach V, Schäfer J, Tobai J, Ridder M, Dreier T, Schaich T et al. Experimental investigation and computational modeling of hot filament diamond chemical vapor deposition. J Chem Phys 1997;107:5918-5928.

[59] Chenevier M, Cubertafon JC, Campargue A, Booth JP. Measurement of atomic hydrogen in a hot filament reactor by two-photon laser-induced fluorescence. Diamond Relat Mater 1994;3(4-6):587-592.

[60] Piazza F, González JA, Velázquez R, De Jesús J, Rosario SA, Morell G. Diamond film synthesis at low temperature. Diamond Relat Mater 2006;15(1):109-116.

[61] Piazza F, Morell G. Synthesis of diamond at sub 300 C substrate temperature. Diamond Relat Mater 2007;16(11):1950-1957.

[62] Piazza F, Solá F, Resto O, Fonseca LF, Morell G. Synthesis of diamond nanocrystals on polyimide film. Diamond Relat Mater 2009;18(2-3):113-116.

[63] Piazza F, Morell G, Beltran-Huarac J, Paredes G, Ahmadi M, Guinel M. Carbon nanotubes coated with diamond nanocrystals and silicon carbide by hot-filament chemical vapor deposition below 200 C substrate temperature. Carbon 2014;75, 113-123.

[64] Piazza F. Carbon nanotubes conformally coated with diamond nanocrystals or silicon carbide, methods of making the same and methods of their use. U.S. Patent 9,458,017, 2016.

[65] Wagner J, Wild C, Koidl P. Resonance effects in Raman scattering from polycrystalline diamond films. Appl Phys Lett 1991;59(7):779-781.

[66] Regan W, Alem N, Aleman B, Geng B, Girit C, Masareti L et al. A direct transfer of layer-area graphene. Appl Phys Lett 2010;96:113102-1-113102-3.

[67] Kresse G, Hafner J. Ab initio molecular dynamics for liquid metals. Phys Rev B 1993;47:558-561.

[68] Kresse G, Furthmüller J. Efficient iterative schemes for *ab initio* total-energy calculations using a plane-wave basis set. Phys Rev B 1996; 54: 11169-11186.

[69] Blöchl PE. Projector augmented-wave method. Phys Rev B 1994;50:17953-17979.

[70] Kresse G, Joubert D. From ultrasoft pseudopotentials to the projector augmented-wave method. Phys Rev B 1999; 59: 1758-1775.

[71] Perdew JP, Burke K, Ernzerhof M. Generalized Gradient Approximation Made Simple. Phys Rev Lett 1996;77:3865-3668.

[72] Hedin L. New Method for Calculating the One-Particle Green's Function with Application to the Electron-Gas Problem. Phys Rev 1965; 139:A796- A823.

[73] Shishkin M, Kresse G. Implementation and performance of the frequency-dependent GW method within the PAW framework. Phys Rev B 2006;74: 035101-035113.

[74] Heyd J, Scuseria GE. Assessment and validation of a screened Coulomb hybrid density functional. J Chem Phys 2004; 120: 7274-7280.

[75] Paier J, Marsman M, Hummer K, Kresse G, Gerber IC, Ángyán JA, Screened hybrid density functionals applied to solids. J Chem Phys 2006; 124: 154709-154713.

[76] Togo A, Tanaka I, First principles phonon calculations in materials science, Scripta Materialia 2015;108: 1–5.

[77] Casiraghi C, Raman Spectroscopy of graphene. In: Yarwood J, Douthwaite R, Duckett S, editors. Spectroscopic Properties of Inorganic and Organometallic Compounds: Techniques, Materials and Applications, vol. 43, Royal Society of Chemistry; 2012 p. 29-56.

[78] Eckman A, Felten A, Mishchenko A, Britnell L, Krupke R, Novoselov KS et al. Probing the Nature of Defects in Graphene by Raman Spectroscopy. Nano Lett 2012;12 (8):3925–3930.

[79] Piazza F, Golanski A, Schulze S, Relihan G. Transpolyacetylene chains in hydrogenated amorphous carbon films free of nanocrystalline diamond. Appl Phys Letters 2003;82(3):358-360.

[80] Piazza F, Schulze, Relihan G, Golanski A. Transpolyacetylene chains in DECR plasma deposited aC:H films. Diamond Relat Mater 2003;12(3-7):942-945.

[81] Piazza F., Grambole D, Herrmann F, Relihan G, Barthe MF, Desgardin P, Golanski A. Incorporation of hydrogen and oxygen into (t)a-C:H thin films deposited using DECR plasma. Mat Res Soc Symp Pro 2001;675:W10.3.1-W10.3.6.

[82] Casiraghi C, Piazza F, Ferrari AC, Grambole D, Robertson J. Bonding in hydrogenated diamond-like carbon by Raman spectroscopy. Diamond Relat. Mater 2005;14(3-7):1098-1102.

[83] Tuinstra F, Koenig JL. Raman spectrum of graphite. J Chem Phys 1970;53:1126-1130.

[84] Gilkes KWR, Prawer S, Nugent KW, Robertson J, Sands HS, Lifshitz Y et al. Direct quantitative detection of the sp^3 bonding in diamond-like carbon films using ultraviolet and visible Raman spectroscopy. J Appl Phys 2000;87:7283-7289.

[85] Ferrari AC, Robertson J. Resonant Raman spectroscopy of disordered, amorphous, and diamond-like carbon, Phys Rev B 2001: 64:075414-1-075414-13.

[86] Schügerl FB, Kuzmany H. Optical modes of trans-polyacetylene. J Chem Phys 1981;74(2):953-958.

[87] Prawer S, Nugent KW, Jameieson DN, Orwa JO, Bursill LA, Peng JL. The Raman spectrum of nanocrystalline diamond. Chem Phys Lett 2000; 332:93-97.

[88] Casiraghi C, Ferrari AC, Robertson J. Raman spectroscopy of hydrogenated amorphous carbons. Phys Rev B 2005;72:085401-1-085401-1.

[89] Smith DC, Godard G. UV and VIS Raman spectra of natural lonsdaleites: Towards a recognized standard. Spectrochimica Acta Part A 2009;73:428-435.

[90] Gogotsi YG, Kailer A, Nickel KG. Pressure-induced phase transformations in diamond. J Appl Phys 1998;84:1299-1304.

[91] Spear KE, Phelps AW, White WB. Diamond polytypes and their vibrational spectra. J Mater Res 1990;5(11) 2277-2285.

[92] Knight DS, White WB. Characterization of diamond films by Raman spectroscopy. J Mater Res 1989. 4(2):385-393.

[93] Fox JJ, Martin AE. Investigations of infra-red spectra. Determination of C-H frequencies (~3000 cm-1) in paraffins and olefins, with some observations on "polythenes". Proc R Soc Lond A 1940;175 : 208-233.

[94] Lebègue S, Klintenberg M, Eriksson O, Katsnelson MI. Accurate electronic band gap of pure and functionalized graphane from GW calculations. Phys Rev B 2009; 79(24): 245117–5.

[95] Cudazzo P, Attaccalite C, Tokatly IV, Rubio A. Strong Charge-Transfer Excitonic Effects and the Bose-Einstein Exciton Condensate in Graphane. Phys. Rev. Lett 2010; 104(22): 226804–4.

[96] Karlický F, Otyepka M. Band Gaps and Optical Spectra of Chlorographene, Fluorographene and Graphane from G_0W_0, GW_0 and GW Calculations on Top of PBE and HSE06 Orbitals. J Chem Theory Comput 2013; *9*(9): 4155–4164.

[97] Ager III JW, Veirs DK, Rosenblatt GM. Spatially resolved Raman studies of diamaond films grown by chemical vapor deposition. Phys Rev B 1991;43:6491-6499.

[98] Osswald S, Mochalin VN, Havel M, Yushin G, Gogotsi Y. Phonon confinement effects in the Raman spectrum of nanodiamond. Phys Rev B 2009;80:075419.

[99] Saada D, Adler J, Kalish R. Transformation of diamond (sp^3) to graphite (sp^2) bonds by ion-impact. Int J Modern Phys C 1998. 9:61-69.

[100] Piazza F. U.K. Patent Application Number 1809206.4, 05 June 2018.

[101] Daulton TL. Extraterrestrial Nanodiamonds in the Cosmos. in "Ultra Nanocrystalline Diamond, Synthesis, Properties, and Applications", Edited by Shenderova OA, Gruen DM, William Andrew Publishing, Norwich, New York, U.S.A.

[102] Phelps AW. Interstellar diamond. II. Growth and identification. http://www.lpi.usra.edu/publications/abstracts.shtml:; Lunar Planet. Sci. XXX (1999), Abstract #1753.

[103] Garcia-Hernandez DA, Iglesias-Groth S, Acosta-Pulido JA, Manchado A, Garcia-Lario P, Stanghellini L et al. The formation of fullerenes: clues from new C_{60}, C_{70}, and (possible) planar C_{24} detections in magellanic could planetary nebulae. Astrophysical J Lett 2011;737:L30 (2011).

[104] Zhao L, Kaiser R, Xu B, Ablikin U, Ahmed M, Joshi D et al. Pyrene synthesis in circumstellar envelopes and its role in the formation of 2D nanostructures. Nature Astronomy 2018;2:413-419.